Automated Fabric Defect Detection Based on Multiple Gabor Filters and KPCA

Junfeng Jing[1], Xiaoting Fan[2] and Pengfei Li[3]

[1, 2, 3] *School of Electronic and Information, Xi'an Polytechnic University, Xi'an, 710048, China*
[1]*Jingjunfeng0718@sina.com,* [2]*Fanxiaoting1234@126.com ,* [3]*413066458@qq.com*

Abstract

A new detection approach is proposed to detect various uniform and structured fabric defects based on the multiple Gabor filters and Kernel Principal Component Analysis. First of all, images are filtered by multiple Gabor filters with six scales and four orientations to extract feature vectors. After that, the sub-blocks divided from the feature vectors have been fused and the high-dimension data can be reduced by using Kernel Principal Component Analysis. Finally, the similarity matrix is calculated by Euclidean norm and segmented with OTSU threshold method. The experiment has been done by integrating hardware and NI LabVIEW graphical programming language. Experimental results show that proposed algorithm improves feature extraction capability significantly and has high recognition rate.

Keywords: Defect detection, Multiple Gabor filters, KPCA, LabVIEW

1. Introduction

Nowadays, with the rapid development of computer and image processing technology, computer vision has been widely used in textile industrial production. Therefore, automated fabric defect detection becomes a natural way to improve fabric quality and reduce labor costs [1]. Since 1980s, many researches in the field of fabric defect detection based on computer vision have been widely carried out. In practical application field, defect inspection equipments included Uster's Fabriscan, IQ TEX-4, Barco's Vision Cyclops and German mahlo WEBSCAN WIS-12 [2], but the cost of investments is higher and the enterprise recovery time is longer. Thus, the development of automated fabric defect detection with high accuracy and fast speed seems to be necessary and has profound significance [3].

Many scholars all over the world have proposed various approaches in the fabric defect detection in the past two decades [4-15]. In [4] a new filtering program for unsupervised fabric defect detection utilized a class of self-similar Gabor functions is proposed and a low-cost settlement for the web inspection used the odd part of the Gabor function is presented. Tsai D M *et al*. [5] used a 1-D ring-projection transformation to compress a 2-D grey-level image into a 1-D pattern, then employed a 1-D Gabor filter to detect a homogeneous texture defects. In [6] Gabor filters was used to extract texture features for texture defect, which could automatically segment defects from the regular texture. An optimized ring Gabor filter (RGF) is presented to inspect the small surface defects in texture materials and the parameters of the filter were determined by a simulated annealing (SA) algorithm [7]. Another approach based on the energy response from the convolution of Gabor filters in different frequency and orientation domains is reported in [8]. Bissi L *et al*. proposed an algorithm for automated texture defect detection based on a complex symmetric Gabor filter bank and Principal Component Analysis (PCA) for dimensionality reduction [9]. In [10] a method for speeding up feature extraction based on Kernel Principal Component Analysis (KPCA) is described, which was widely used in

nonlinear feature extraction. Approaches mentioned above in the literatures are mainly based on Gabor filters [11-12] and the KPCA is applied to dimensionality reduction of the feature vectors.

In this paper, we propose a method based on multiple Gabor filters and KPCA, which is used for real-time automated fabric defect detection. Compared with other approaches in fabric defects defection, the main characteristics of the proposed method are as follows: the texture features extraction phase relies on multiple Gabor filters and KPCA is used for nonlinear dimensionality reduction. Then OTSU, a commonly used thresholding technique, is used to detect defects from the background texture. The organization of this paper is as follows: In Section 2, calibration procedure, image inspection and the selection of optimization parameters are reported in defect detection phase. In Section 3, we give a discussion on the experimental results with the proposed algorithm, in order to analyze the results obtained by considering different parameters for the multiple Gabor filters. In Section 4, a computer vision based on automatic inspection system is introduced, which can effectively detect and identify defects on various kinds of fabrics. Some conclusions are drawn in the final section. It is proved that the proposed method is effective for a reflective fabric image with four basic weaving structures, namely, holes, oil spots, thread errors and objects on the surface. The proposed method can reduce the computational time for defect detection and improve the detection success rate significantly.

2. Description of Method

Fabric defect detection processing consists of three parts: a) calibration, b) defect image inspection and c) threshold comparison. Calibration is mainly to prepare for obtaining the relevant parameters which are used to reduce noise of defect images in defect detection. Image features are extracted by multiple Gabor filters, then the filtered images are divided into a large number of non-overlapping sub-blocks. Afterwards, we make data fusion of the corresponding sub-blocks divided from fabric images and the high-dimension data of fused sub-blocks feature vectors is reduced by KPCA, then the median filtering and similarity comparison are operated on the low-dimension feature vectors. Finally, the OTSU's method is used to realize binarization threshold and the binary images can be obtained.

2.1. Image Inspection

The chart diagram of the image inspection algorithm is shown in Figure 1.
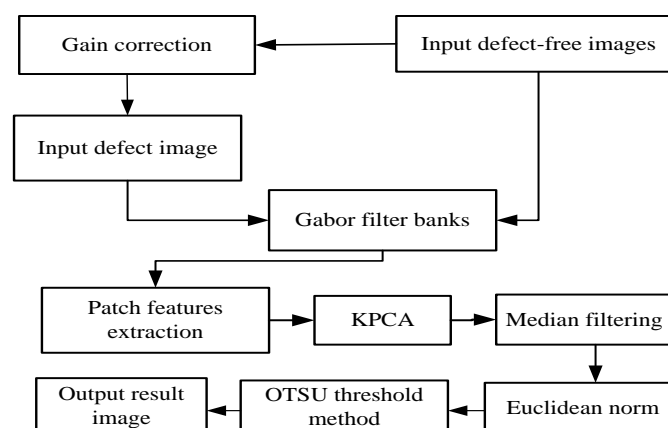
Figure 1. Block Diagram of the Proposed Algorithm

The defect image is represented as $I_a(x,y)$, in size W_1*W_2 pixels. $I(x,y)$, a gain corrected image, is obtained by the product of the defect image $I_a(x,y)$ and the correction gain

$G_{gain}(x,y)$ which can eliminate the impact of image device shooting posture and nonlinear distortion caused by scanning (the gain corrected $G_{gain}(x,y)$ will be shown how to be calculated out in the calibration procedure). The gain corrected image $I(x,y)$ is convolved with the multiple Gabor filters, $f_{i,j}(x,y)$, $i=0,\dots,I$-1, $j=0,\dots,J$-1, where I indicates the number of scales and J indicates the number of rotations [15]. The output image is given by Eq. (1):

$$I_{i,j}(x,y) = \left([f_{i,j}(x,y)_E \cdot I(x,y)]^2 + [f_{i,j}(x,y)_O \cdot I(x,y)]^2\right)^{1/2}$$

(1)

Where "·" denotes 2-D convolution operation, $f_{i,j}(x,y)_E$ and $f_{i,j}(x,y)_O$ represent the even (sine-type) part and odd (cosine-type) part of the Gabor filter, respectively.

In the spatial domain, the Gabor function is a complex exponential modulated by a Gaussian function, which forms a complete but a non-orthogonal basis set. It's an impulse response in the 2-D plane, which has the following general formula [16]:

$$f(x,y) = \frac{1}{2\pi\sigma_x\sigma_y}\exp\left[-\frac{1}{2}\left(\frac{x^2}{\sigma_x^2} + \frac{y^2}{\sigma_y^2}\right)\right] * \exp(2\pi jw_0 x)$$

(2)

$$\sigma_x = \frac{\sqrt{2\ln 2}(a+1)}{2*pi*(a-1)}, \sigma_y = \left[2\ln 2 - \left(\frac{2\ln 2}{2*pi*\sigma_x*w_j}\right)\right]^{1/2} * \left[2*pi*\tan\left(\frac{pi}{2}\right)\left(w_j - 2\ln\left(\frac{1}{4*pi^2*\sigma_x*w_j}\right)\right)\right]^{-1}$$

(3)

Where the space contains σ_x and σ_y define the Gaussian envelope along the x and y axes, the w_0 denotes the radial center frequency and w_j denotes the lowest frequency of the Gabor function. The Figure 2 shows the even part and the odd part of the responses of a basic Gabor function.
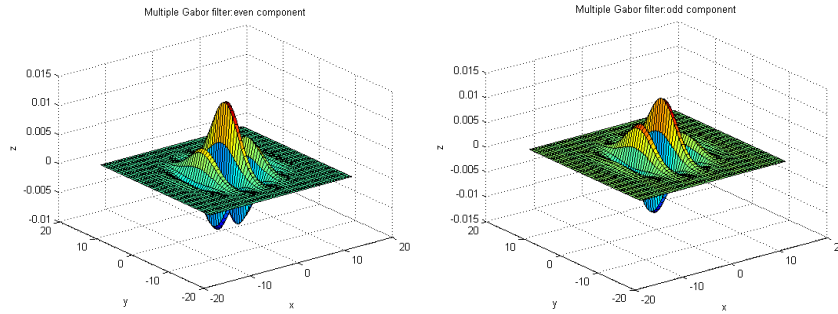
Figure 2. Perspective View of (a) Even and (b) Odd Parts of a Typical Gabor Function

A class of self-similar functions, referred to as Gabor wavelets, which have been used for texture analysis [16]. Using Eq.(2) as the mother Gabor wavelet, the self-similar filter functions can be obtained by appropriate scale transformation and rotation transformation of $f(x,y)$ through the generating function.

$$f_{i,j}(x,y) = a^{-j} * f(x',y')$$

(4)

Where, $x' = a^{-j} * (x*\cos\theta_i + y*\sin\theta_i)$, $y' = a^{-j} * (-x*\sin\theta_i + y*\cos\theta_i)$

$$\theta_i = (i*pi)/I, a = (w_j/w_0)^{-(1/(j-1))} (i=0,\dots,I-1, j=0,\dots,J-1, a\geq 2)$$

The integer subscripts i and j represent the index for scale (dilation) and rotation (orientation), respectively. The scale factor a^{-j} ensures that all the Gabor filters have the same energy, regardless of the scales and orientations. The frequency and orientation half-peak bandwidths are defined as follows, respectively [16].

$$D = \log_2\left[\left(2*pi*w_j*\sigma_x + 2\ln 2\right)/\left(2*pi*w_j*\sigma_x - 2\ln 2\right)\right], \gamma = 2\tan^{-1}\left[\left(2\ln 2/2*pi*w_j*\sigma_x\right)\right]$$

The angle of the 2-D frequency plane is divided into six different scales (I=6) and four

Orientations ($J=4$) [17]. The radial center frequency of the Gabor function is chosen by experiences. In general, larger defects require a lower filter radial center frequency. The model with circular symmetry of the Gaussian section is considered, $\sigma_x = \sigma_y = \sigma$. In order to achieve higher detection performance, each Gabor filter includes a kernel size l of 9*9 and the scale factor a^{-j} ($a=2$) are selected. These values are selected based on the methods mentioned in previous articles [1, 2, 9].

Afterwards, defect fabric images at each filter outputs $I_{i,j}(x,y)$ are divided into $M=C_1*C_2$ non-overlapping blocks of m_1*m_2 pixels, where $C_1=W_1/m_1$ and $C_2=W_2/m_2$, and the filtered images

$I_{i,j}(x,y)$ are divided into blocks of 16*16 pixels in this paper, same as [18]. In view of the experiments are executed by using defect-free and defect fabric images taken from TILDA Textile Texture Database [18], so $C_1=768/16=48$, $C_2=512/16=32$ and $M=48*32=1536$. The corresponding sub-blocks of each Gabor filter outputs $I_{i,j,m}(x,y)$, $m=1,\ldots,M$, are spliced in data fusion. After splicing, each matrix block is defined as a feature vector $f_{ed}(d_1,d_2)$ of dimension (m_1*m_2*I*J), where $d_1=1,\ldots,C_1$, $d_2=1,\ldots,C_2$, namely, $m_1*m_2*I*J=6144$. Then, KPCA is performed by using covariance matrix, which can reduce the dimension of the feature vectors down to R (the dimension is reduced to $R=128$ in this paper).

PCA [19] algorithm is a linear method for dimensionality reduction. KPCA is an improved PCA, which can extract principal components by adopting a nonlinear kernel method [20-22]. KPCA maps the high dimension features in the input space to a new lower dimension eigenspace via a nonlinear mapping. Then the linear PCA is performed to find a set of eigenvectors that are nonlinearly related to the input data. Assuming training samples $m_1, m_2, \ldots, m_k$ and $\{M_i\}$ represents the input vector space and $\varphi(m)$ represents the nonlinear mapping. The eigenvalues and eigenvectors of the nuclear matrix

$$C = 1/K \sum_{i=1}^{K} \varphi(m_i)\varphi(m_i)^T (X \times X)$$ can be calculated via using

$Cv = \lambda v$, where λ is one of the eigenvalues of C and v is the corresponding eigenvector. Eigenvalues normalized obtained by $v_c^T v_c = 1/\lambda_c$, $c=1,2,\ldots,q$, where λ_q are the smallest non-zero eigenvalues that in descending order. The principal component test points are extracted to calculate the projection,

$$f_c(m) = v_c \times \varphi(m) = \sum_{i=1}^{X} v_i^c (\varphi(m_i) \times \varphi(m)) = \sum_{i=1}^{X} v_i^c C(m_i,m),$$ where $c=1,2,\ldots,q$,

a_i^c is the ith of eigenvector a^c.

Accordingly, a single image can be represented by the sub-blocks feature vectors reduced. $f_{kpca}(d_1,d_2,r)$ represents the significant components of the Gabor filtered image, where $d_1=1,\ldots,C_1$, $d_2=1,\ldots,C_2$, $r=1,\ldots,R$. In order to decrease the effect of noise, average reference feature vectors obtained by the defect-free images, $f_{kpca}'(d_1,d_2,r)$ is considered (in the calibration procedure we will show how to calculate out these average features). Afterwards, the Euclidean norm of local feature vectors is calculated [23] by the following formula, respectively:

$$N_{orm}(d_1,d_2) = f_{kpca}(d_1,d_2,r) - f_{kpca}'(d_1,d_2,r) \qquad (5)$$

And a matrix $N_{orm}(d_1,d_2)$ of dimension C_1*C_2 represents all the sub-blocks of the image is

Obtained. It should be underlined that, differently from [24], norm-1 has been used. In order to distinguish the defect area from the fabric image, a threshold T_e is calculated to generate a binary mask of defects, where '0' denotes a defected blocks:

$$B(d_1,d_2) = \begin{cases} 255 & if \ N_{orm}(d_1,d_2) \leq T_e \\ 0 & if \ N_{orm}(d_1,d_2) > T_e \end{cases}$$

$$(6)$$

In order to highlight the defect positions on the defect image, the original image $I_a(x,y)$ and the binary mask image $B(d_1,d_2)$ are made image fusion finally, where each point of the mask image $B(d_1,d_2)$ corresponds to a rectangular patch of m_1*m_2 pixels.

2.2. Calibration Procedure

A number of W defect-free images $I_w(x,y)$, $w=0,\ldots,$ W-1, are smoothed and averaged with a 3*3 Gaussian filter $G_{guass}(x,y)$, in order to get relevant gain correction $G_{gain}(x,y)$ (Figure 3(a)). The corresponding spatially variant gain is applied to all images to maintain the same luminance level, $G_{gain}(x,y)$ is obtained by Eq.(7) and Eq.(8):

$$P(x,y) = \frac{1}{W} \left(\sum_{l=0}^{W-1} I_w (x,y) \right) \cdot G_{guass}(x,y) \tag{7}$$

$$G_{gain}(x,y) = P_{ping} / P(x,y) \tag{8}$$

Where P_{ping} is the average luminance value of the averaged image $P(x,y)$. Three-dimensional diagram of the smoothed and averaged image (Figure 3(b)) shows an uneven lighting, owing to the defectives and dust spots of the camera lens and sensor.

(a)   (b)
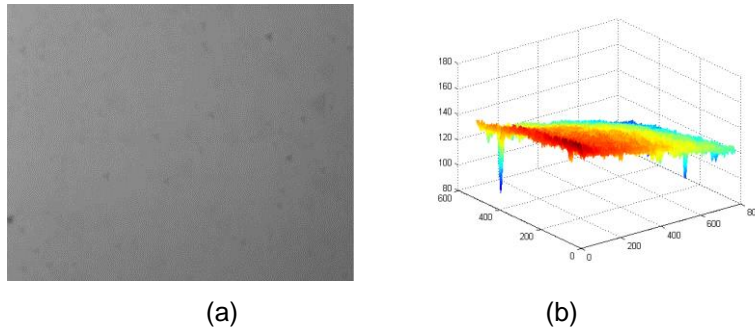
Figure 3. (a) Relevant Correction Gain Image $G_{gain}(X,Y)$ and (b) Smoothed and Averaged Image Luminance $P(X,Y)$

The value of the vectors $f_{kpca}{}'(d_1,d_2,r)$ is also calculated by the defect-free images $I_w(x,y)$, $w=0,\ldots,W$-1, instead of a single image, as done in [16,25].The tasks described in image inspection of the defect detection processing (Figure 1) are applied to the defect-free images: multiple Gabor filters, image segmentation, data fusion and KPCA. Then, the reduced feature vectors $f_{kpca}{}'^t(d_1,d_2,r)$ of dimension R are obtained, the average matrix $f_{kpca}{}'(d_1,d_2,r)$ is defined as:

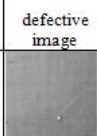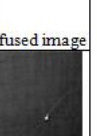$$f_{kpca}{}'(d_1,d_2,r) = \frac{1}{W} \sum_{w=0}^{w-1} f_{kpca}{}'^t(d_1,d_2,r) \tag{9}$$
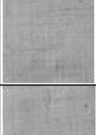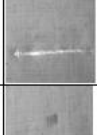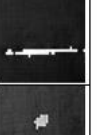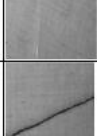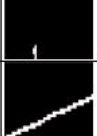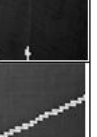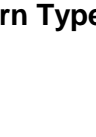
After calculating the Euclidean norm of each matrix, each element of the similarity matrices $N_{orm}(d_1,d_2)$ is compared with a variable threshold value, T_e, obtained by OTSU [26]. OTSU's method is regarded as one of the best threshold selection approaches for fabric images, which is based on discriminant analysis that maximizes some measures of class separability. It assumes that the image contains two classes of pixels: foreground and background, then the optimum threshold is calculated to separate those two classes to minimize the probability of the error. The optimal threshold T_e is used to obtain the binary images finally.

3. Experiments Results and Analysis

To demonstrate the effectiveness of the proposed algorithm in this paper, which has been implemented in MATLAB R2008a and Windows 7 Operating System, Intel(R) Core(TM) i5-2400M Dual Core Processor CPU 4GB 3.10GHz RAM. Experiments are

executed by using defect-free and defect fabric images taken from TILDA Textile Texture Database [18]. The textile group C1 contains uniformly textured, thin materials and the textile group C2 contains visible texture, grid-like structure. Four classes defects consist of holes (E1), oil spots (E2), thread errors (E3) and objects on the surface (E4). A defect-free reference class (E0) is also defined. 50 images are reported for each class, of dimension 768*512. Then the algorithm is applied to all the images with defects of the classes E1-E4 of C1 yarn types and the classes E1-E4 of C2 yarn types.

Parts of consequences of C1 yarn types are shown in Figure 4 include defect-free images, defect images, binary images and fused images. Detection results of C2 with the same type defect images are exhibited in Figure 5. Parameters of test images in Figure 4 and Figure 5 with different scales and rotations are reported in Table 1.

Name	The number in the TILDA Textile Texture Database	Defect Types	defect-free image	defective image	binary image	fused image
a	C1R1EABS	holes				
b	C1R1EACP	holes				
c	C1R1E2N3	oil spots				
d	C1R1EADR	oil spots				
e	C1R1EAHZ	thread errors				
f	C1R1E4N1	objects on the surface				
g	C1R1E4N7	objects on the surface				

Figure 4. Examples of Defect Image Belonging to E1-E4 Error Classes of C1 Yarn Type

Figure 5. Examples of Defect Image Belonging to E1-E4 Error Classes of C2 Yarn Types

Table 1. Parameters of Multiple Gabor Filters of all Images in Figure 4 and Figure 5

	I=6, J=4		I=6, J=5		
	σ T_e	t	σ	t	T_e
Figure4 (a)	3.23 9.7377	22.88	6.47 6.1928	25.38	
Figure4 (b)	3.23 2.7564	23.08	6.47 2.8869	24.48	
Figure4 (c)	3.23 4.9937	18.88	6.47 6.3246	23.42	
Figure4 (d)	3.23 6.2778	18.93	6.47 7.0330	22.92	
Figure4 (e)	3.23 7.3871	19.09	6.47 8.5712	23.39	
Figure4 (f)	3.23 3.1230	18.75	6.47 2.4784	22.98	
Figure4 (g)	3.23 5.3251	18.85	6.47 6.3256	22.05	
Figure5 (h)	2.87 17.4849	23.02	5.75 21.0243	27.95	

Figure5 (i)	2.87	23.00	11.9172	5.75	27.66	12.7426
Figure5 (j)	2.87	23.45	8.5612	5.75	27.90	9.6219
Figure5 (k)	2.87	22.85	15.0027	5.75	30.09	15.4018
Figure5 (l)	2.87	23.04	24.7221	5.75	27.94	6.2521
Figure5 (m)	2.87	23.24	10.0729	5.75	28.01	9.9467
Figure5 (n)	2.87	23.95	15.6235	5.75	27.54	13.2654

From Table 1, it can be seen that the σ is determined by the radial center frequency w_0 and the kernel size l for C1 and C2 yarn types, here, $w_0=1/32$, $l=9*9$ for fabrics in Figure 4 and $w_0=1/36$, $l=11*11$ for fabrics in Figure 5 are chosen, respectively. In the above cases, for C1 and C2 yarn types, the algorithm with $I=6$, $J=4$ gives better results than $I=6$, $J=5$, the lower number of orientations plays a positive role and takes a relatively shorter detection time. In terms of the detection time and the range of threshold: the class of uniformly textured and thin materials takes shorter time and lower threshold than the class of visible texture and grid-like structure. In other words, more scales or orientations cannot be used to improve the effectiveness of the algorithm.

There are two ways to measure the accuracy of detection a) detection success rate or b) specificity and sensitivity [27]. Generally, detection success rate, also known as detection accuracy, is defined as

$$detection\ success\ rate = \frac{number\ of\ samples\ corrctly\ detected}{total\ number\ of\ samples}$$

Therefore, fabric detection rate of the proposed algorithm obtained with the images of the TILDA textile group C1 and C2 yarn types are reported in Table 2.

Table 2. Fabric Detection Rate of the Proposed Algorithm Obtained with the Images of the TILDA Textile Group C1 and C2 Yarn Types

Detection results	E1-E4 of C1				E1-E4 of C2			
	Hole	Oil spots	thread errors	objects on the surface	Hole	Oil spots	thread errors	objects on the surface
Overall detection	(50/50) 100%	(50/50) 100%	(50/50) 100%	(50/50) 100%	(50/50) 100%	(50/50) 100%	(50/50) 100%	(50/50) 100%
True detection	(48/50) 96%	(47/50) 94%	(48/50) 96%	(46/50) 92%	(46/50) 92%	(48/50) 96%	(48/50) 96%	(45/50) 90%
False detection	(2/50) 4%	(3/50) 6%	(2/50) 4%	(4/50) 8%	(4/50) 8%	(2/50) 4%	(2/50) 4%	(5/50) 10%

The results listed in Table 2 show that the false detection rate of hole, oil spot, thread errors, objects on the surface belonging to E1-E4 of C1 are 4%,6%,4%,8% and E1-E4 of C2 are 8%, 4%, 4%, 10%. These results indicate that the proposed algorithm achieves better performance in terms of false detection rate. The true detection rate of hole and thread errors belonging to E1-E4 of C1 increases up to 96%, and the true detection rates of oil spots and thread errors belonging to E1-E4 of C2 increases up to 96%. In general, our algorithm performs better in almost all cases for thread errors type.

Table 3 outlines definitions of true negative (*tn*), false negative (*fn*), false positive (*fp*), true positive (*tp*) in defect detection. So detection success rate can also be defined as

$$detection\ success\ rate = \frac{tn + tp}{tn + fp + tp + fn}$$

On the other hand, specificity and sensitivity can be defined as

$$specificity = \frac{tn}{fp + tn}, \quad sensitivity = \frac{tp}{tp + fn}$$

Table 3. Definitions of True Positive, False Positive, True Negative, False Negative in Defect Detection

	Actually defect-free	Actually defective
Detected as defect-free	True negative (*tn*)	False negative (*fn*)
Detected as defective	False positive (*fp*)	True positive (*tp*)

Correct detection of defective samples (*i.e.* sensitivity), correct detection of defect-free samples (*i.e.* specificity) and detection success rate are reported for C1 and C2 yarn types in Figure 6. Detection rate of the proposed algorithm under different parameters, such as GL-2, GL-1, GI=4,J=3, GI=3,J=4, GI=4,J=4, GI=3,J=3, GEv, GOd applied to E1-E4 of C1 are reported in Table 5, where GL-2: Euclidean norm, GL-1: Norm-1 instead of Euclidean norm; GI=4,J=3: I = 4 and J = 3; GI=3,J=4: I = 3 and J = 4; GI=4,J=4: I= 4 and J = 4; GI=3,J=3: I = 3 and J = 3; GEv: Even part of Gabor filters only; GOd: Odd part of Gabor filters only.
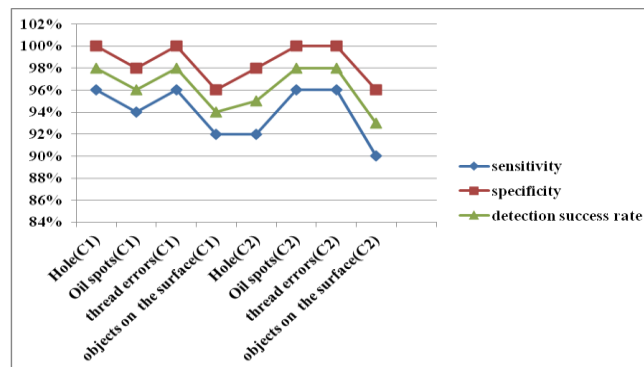
Figure 6. Sensitivity, Specificity and Detection Success Rate of C1 and C2 Yarn Types

Table 5. Detection Rate of $G_L{}^{-2}$, $G_L{}^{-1}$, $G_{I=4,J=3}$, $G_{I=3,J=4}$, $G_{I=4,J=4}$, $G_{I=3,J=3}$, G_{Ev}, G_{Od} Applied to C1

Detection rate images	$G_{L^{-2}}$	$G_{L^{-1}}$	$G_{I=4,J=4}$	$G_{I=3,J=4}$	$G_{I=4,J=3}$	$G_{I=3,J=3}$	G_{Ev}	G_{Od}
Oil spots	(47/50) 94%	(48/50) 96%	(42/50) 84%	(41/50) 82%	(45/50) 90%	(40/50) 80%	(42/50) 84%	(40/50) 80%
Hole	(48/50) 96%	(45/50) 90%	(40/50) 80%	(40/50) 80%	(46/50) 92%	(38/50) 76%	(40/50) 80%	(42/15) 84%
Thread errors	(48/50) 96%	(43/50) 86%	(40/50) 80%	(42/50) 84%	(48/50) 96%	(40/50) 80%	(42/50) 84%	(42/50) 84%
Objects on the surface	(46/50) 92%	(45/50) 90%	(45/50) 90%	(42/50) 84 %	(44/50) 88%	(42/50) 84%	(44/50) 88%	(44/50) 88%

Table 5 is conducted to evaluate the true detection rate of algorithm with different parameters. The results in the first column and second column are compared to verify the effect of norm operation on the algorithm performance, for example, Euclidean norm algorithm can significantly improve the true detection rate from 86% to 96% for thread errors. Comparisons of different scales and orientations are shown in the third to the sixth column, obviously, for C1 yarn type, the algorithm with $I=4$, $J=3$ gives the best performance and $I=3$, $J=3$ gives the worst performance. In general, the higher number of scales have a better detection performance. The results of the last two columns are merely considering the effect of the even and odd part of multiple Gabor filters and they have similar true detection rate.

4. Automation for Inspection

4.1. Acquisition System Hardware Selection and Design

Generally speaking, the real-time fabric defect detection system is divided into two systems: hardware architecture and software system. A front view of the architecture of a typical automated textile web inspection system is shown in Figure 7.

In this system, the LS-MECAPION Company's 24V DC servo motors are selected. Two BASLER L304 cameras produced in the BASLER Company and the Nikon's AF Nikkor 50f/1.8D lens are used to achieve the acquisition of fabric images. High-precision NI-1430 image capture card and the OPT-APA6024-2 series of LED light source are selected. The LabVIEW software combined with the hardware architecture chooses the location and size of collected images.

Figure 7. A Front View of the Architecture of a Typical Automated Textile Web Inspection System

4.2. LabVIEW Graphical User Interface Design

Fabric defect detection based on LabVIEW with the proposed algorithm is applied to fabric processing. The LabVIEW user interface is shown in Figure 8 and the main characteristic of this GUI is image acquisition and image processing window.
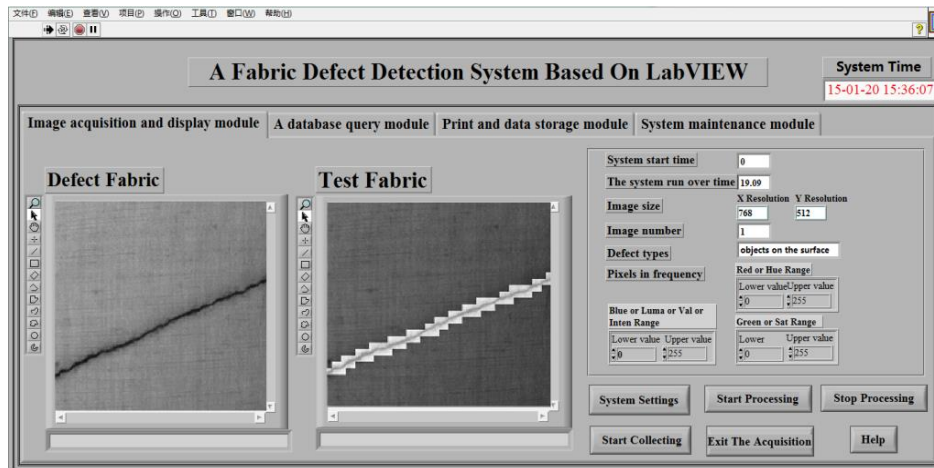

Figure 8. Front Panel of Image Acquisition and Processing

5. Conclusion

In this paper, a supervised defect detection approach to detect a class of fabric defects has been demonstrated. The performance of the proposed approach based on multiple Gabor filters and KPCA has been evaluated by utilizing fabric images of the TILDA Textile Texture Database. The multiple Gabor filters have been used to extract texture features and KPCA has been used for nonlinear dimensionality reduction to achieve more accurate fabric defect detection. In the proposed approach, the true detection rate of the basic algorithm has been tested. Some optimization solutions have been compared with each other and the optimal operational parameters for four kinds of defect yarn types have been found. The tests conducted on different types of defects and different kinds of fabrics have yielded promising results, which have shown that this method achieves a high true detection rate and a low cost for online fabric inspection successfully.

Acknowledgements

References

[1] A. Kumar, "Computer-vision-based fabric defect detection: a survey", Industrial Electronics, IEEE Transactions on, vol. 55, no. 1, **(2008)**, pp. 348-363.

[2] L. Bissi, G. Baruffa and P. Placidi, "Automated defect detection in uniform and structured fabrics using Gabor filters and PCA", Journal of Visual Communication and Image Representation, vol. 24, no. 7, **(2013)**, pp. 838-845.

[3] T. L. Su and C. F. Lu, "Automated vision system for recognising Lycra Spandex Defects", Fibres & Textiles in Eastern Europe, vol. 19, no. 1, **(2011)**, pp. 43-46.

[4] Y. Xu, D. Zhang and F. Song, "A method for speeding up feature extraction based on KPCA", Neurocomputing, vol. 70, no. 4, **(2007)**, pp. 1056-1061.

[5]   D. M. Tsai and C. P. Lin, "Fast defect detection in textured surfaces using 1D Gabor filters", the international journal of advanced manufacturing technology, vol. 20, no. 9, **(2002)**, pp. 664-675.

[6]   J. Jing, H. Zhang and J. Wang, "Fabric defect detection using Gabor filters and defect classification based on LBP and Tamura method", Journal of The Textile Institute, vol. 104, no. 1, **(2013)**, pp. 18-27.

[7]   G. H. Hu, "Optimal ring Gabor filter design for texture defect detection using a simulated annealing algorithm", Information Science, Electronics and Electrical Engineering (ISEEE), 2014 International Conference on. IEEE, vol. 2, **(2014)**, pp. 860-864.

[8]   Y. Shu and Z. Tan, "Fabric defects automatic detection using gabor filters", Intelligent Control and Automation, WCICA 2004. Fifth World Congress on IEEE, vol. 4, **(2004)**, pp. 3378-3380.

[9]   L. Bissi, G. Baruffa and P. Placidi, "Patch based yarn defect detection using Gabor filters", Instrumentation and Measurement Technology Conference (I2MTC), 2012 IEEE International. IEEE, **(2012)**, pp. 240-244.

[10] H. M. Ebied, "Feature extraction using PCA and Kernel-PCA for face recognition", Informatics and Systems (INFOS), 2012 8th International Conference on. IEEE, MM-72-MM-77, **(2012)**.

[11] L. L. Shen and L. Bai, "Gabor feature based face recognition using kernel methods", Automatic Face and Gesture Recognition, 2004. Proceedings. Sixth IEEE International Conference on. IEEE, **(2004)**, pp. 170-176.

[12] M. R. Swati and M. Ravishankar, "Finger Knuckle Print recognition based on Gabor feature and KPCA+ LDA", Emerging Trends in Communication, Control, Signal Processing & Computing Applications (C2SPCA), 2013 International Conference on. IEEE, **(2013)**, pp. 1-5.

[13] M. Ralló, M. S. Millán and J. Escofet, "Unsupervised novelty detection using Gabor filters for defect segmentation in textures", JOSA A, vol. 26, no. 9, **(2009)**, pp. 1967-1976.

[14] H. Y. T. Ngan, G. K. H. Pang and N. C. H. Yung, "Automated fabric defect detection a review", Image and Vision Computing, vol. 29, no. 7, **(2011)**, pp. 442-458.

[15] C. W. Li and D. M. Tsai, "Wavelet-based defect detection in solar wafer images with inhomogeneous texture", Pattern Recognition, vol. 45, no. 2, **(2012)**, pp. 742-756.

[16] D. Dunn, W. E. Higgins and J. Wakeley, "Texture segmentation using 2-D Gabor elementary functions", Pattern Analysis and Machine Intelligence, IEEE Transactions on, vol. 16, no. 2, **(1994)**, pp. 130-149.

[17] T. Weldon and W. E. Higgins, "Designing multiple Gabor filters for multitexture image segmentation", Optical Engineering, vol. 38, no. 9, **(1999)**, pp. 1478-1489.

[18] A. Basturk, H. Ketencioglu and Z. Yugnak, "Inspection of defects in fabrics using Gabor wavelets and principle component analysis", Signal Processing and Its Applications, 2007. ISSPA 2007. 9th International Symposium on. IEEE, **(2007)**, pp. 1-4.

[19] M. Eldessouki, M. Hassan and K. Qashqari, "Application of Principal Component Analysis to Boost the Performance of an Automated Fabric Fault Detector and Classifier", FIBRES & TEXTILES in Eastern Europe, vol. 22, no. 4, 106, **(2014)**, pp. 51-57.

[20] A. B. Musa, "A comparison of ℓ1-regularizion, PCA, KPCA and ICA for dimensionality reduction in logistic regression", International Journal of Machine Learning and Cybernetics, 2014, 5(6): 861-873.

[21] Z. Chen, H. Ren and X. Du, "Minimax probability machine classifier with feature extraction by kernel PCA for intrusion detection", Wireless Communications, Networking and Mobile Computing, 2008. WiCOM'08. 4th International Conference on. IEEE, **(2008)**, pp. 1-4.

[22] M. Ding, Z. Tian and H. Xu, "Adaptive kernel principal analysis for online feature extraction", Proceeding World Acad. Sci., Eng. Technol, vol. 59, **(2009)**, pp. 288-293.

[23] M. E. Celebi, F. Celiker and H. A. Kingravi, "On Euclidean norm approximations", Pattern Recognition, vol. 44, no. 2, **(2011)**, pp. 278-283.

[24] M. Barni, V. Cappellini and A. Mecocci, "Fast vector median filter based on Euclidean norm approximation", Signal Processing Letters, IEEE, vol. 1, no. 6, **(1994)**, pp. 92-94.

[25] L. Shen and L. Bai, "A review on Gabor wavelets for face recognition", Pattern analysis and applications, Moghaddam R F, Ch, vol. 9, no. 2-3, **(2006)**, pp. 273-292.

[26] R. F. Moghaddam and M. Cheriet, "AdOtsu: An adaptive and parameterless generalization of Otsu's method for document image binarization", Pattern Recognition, vol. 45, no. 6, **(2012)**, pp. 2419-2431.

[27] H. Y. T. Ngan, G. K. H. Pang and N. H. C. Yung, "Automated fabric defect detection a review", Image and Vision Computing, vol. 29, no. 7, **(2011)**, pp. 442-458.

Authors

Junfeng Jing, he received the B.S. and M.S. degree in electrical engineering from Xi'an Polytechnic University, Xi'an, Shanxi, China in 2003 and 2006, respectively. Since 2006, he has worked in the School of Electronic and Information, Xi'an Polytechnic University. Since 2009, he has been studying for a doctor's degree in the School of Electronical and Machanical Engineering, Xidian University, Xi'an, Shanxi, China.

Xiaoting Fan, she was born in Heilongjiang, China, in 1991. She received the B.S. degree in electrical engineering from Xi'an Polytechnic University, Xi'an, Shanxi, China in 2014. She is currently studying for a master of science's degree in Xi'an Polytechnic University, Her current research interests include image processing and pattern recognition.
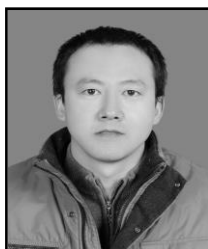
Pengfei Li, he was born in 1962, and graduated in Xi'an Polytechnic University, and is professor in Xi'an Polytechnic University now. His present research interests include machine vision, industrial inspection and so on.